14th International Symposium on Turbulence and Shear Flow Phenomena (TSFP14)
Heidelberg, Germany, July 28–31, 2026

THERMAL BOUNDARY LAYER DEVELOPMENT OVER STEP CHANGE IN SURFACE ROUGHNESS

Shilpa Vijay
Center for Turbulence Research
Stanford University
Stanford, CA
shilpavi@stanford.edu

Beverley J. McKeon
Center for Turbulence Research
Stanford University
Stanford, CA
bjmckeon@stanford.edu

ABSTRACT

Surface roughness significantly influences heat and momentum transfer in engineering flows, yet their coupled behavior under non-equilibrium conditions remains less well understood. Recent direct numerical simulations indicate that the scalar field requires a substantially longer streamwise fetch than the momentum field to recover to equilibrium following a step change in surface condition (MacDonald, 2024), motivating spatially resolved experimental measurements of the thermal recovery region. Specifically, this study investigates thermal boundary layer evolution over step changes in surface roughness using a modular heated-wall system in a low-speed wind tunnel. The facility enables precise control of wall heating, while infrared thermography (IR) provides spatially resolved surface temperature footprints. The streamwise wall-temperature evolution provides a surface-based indicator of thermal internal boundary layer development. These findings highlight the role of surface heterogeneity in sustaining non-equilibrium scalar–momentum coupling.

INTRODUCTION

Many engineering applications, such as flow over canopies, iced airfoils, or damaged turbine blades (Kadivar *et al.*, 2021), involve irregular roughness across a wide range of scales that introduces strong spatial heterogeneity. Of particular interest are abrupt surface changes, such as transitions in roughness or heating, which drive boundary layers into non-equilibrium states characterized by the formation of an internal boundary layer (IBL), that grows downstream of the change while the outer flow retains upstream history. The development of this IBL governs how rapidly the flow adjusts to the new surface condition, and its growth rate sets the streamwise distance over which the wake of the upstream surface remains observable. When the surface change involves both roughness and heating, the problem becomes one of coupled momentum and scalar adjustment, with each governed by an internal boundary layer that may grow at different rates.

In these spatially developing flows, the classical diffusion analogy (Miyake, 1965) fails because scalar transport relies primarily on diffusive processes and form-induced fluxes, whereas momentum transport benefits from pressure-driven enhancement through form drag. Consequently, scalar IBLs exhibit systematically larger growth exponents than their momentum counterparts (Rouhi *et al.*, 2019; MacDonald, 2024), making scalar recovery less understood in such non-equilibrium conditions. Jensen & Forooghi (2025) further showed that patchy roughness generates secondary motions and internal boundary layers whose recovery depends on the size and spacing of rough and smooth patches, highlighting the role of surface heterogeneity and patterning in non-equilibrium turbulence. It remains unclear how the history effects observed in velocity fields under varying pressure gradients may also manifest in temperature fields. Resolving such effects numerically is further complicated by the need to account for conjugate heat transfer (CHT) at the fluid–solid interface. This is typically idealised as iso-flux or iso-thermal in DNS but has been shown to reduce the thermal roughness function by approximately 30% over irregular roughness when properly resolved (Stroh *et al.*, 2025). Surface-resolved experiments inherently capture this coupling and provide a direct method for characterising scalar transport over realistic engineering rough walls.

Experimentally resolving the development of a scalar IBL after a surface transition has remained challenging, in large part because the streamwise evolution of the scalar field is difficult to capture with wall-normal point measurements alone. Infrared thermography offers a complementary approach: by mapping the surface temperature field at high spatial resolution, it provides a wall-resolved, non-intrusive measurement of the thermal footprint that the scalar IBL leaves on the wall as it develops. The persistence of such footprints over several boundary-layer thicknesses downstream of roughness transitions has been linked to the slow recovery of large-scale outer-layer motions, which retain upstream history far longer than small near-wall scales (Li *et al.*, 2019). Such structures carry thermal signatures through the strong coupling between velocity and temperature fluctuations near the wall (Abe *et al.*, 2004). Recent work by Foroozan *et al.* (2025) has demonstrated that infrared thermography can resolve the wall im-

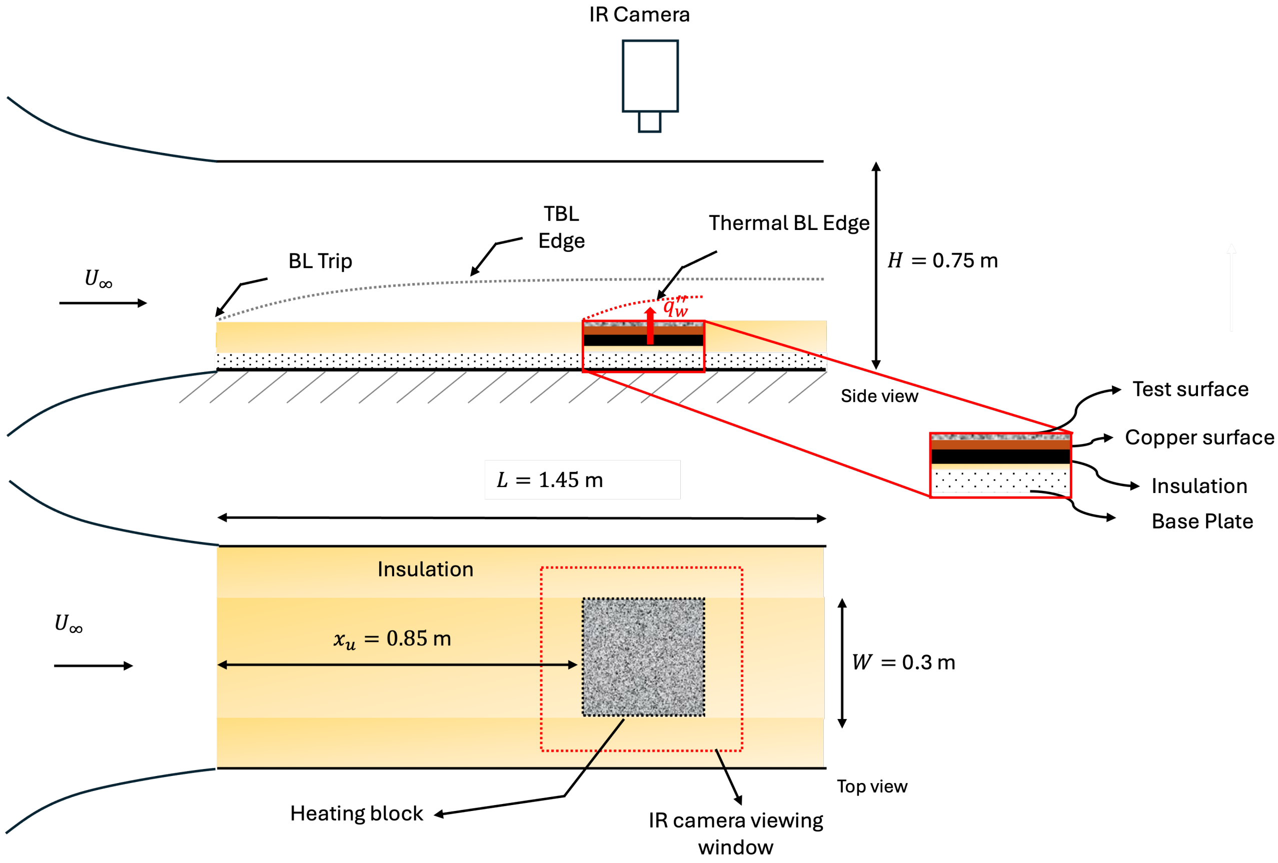

Figure 1: Schematic of the experimental setup in the wind tunnel.

print of velocity structures across multiple wall-normal scales, motivating the use of wall-based thermal measurements as an indirect probe of such interactions. The present study experimentally investigates the development of a thermal internal boundary layer downstream of a heated rough patch transitioning to an unheated smooth surface. A modular heated-wall system generates controlled rough-to-smooth and heated-to-unheated transitions, while infrared thermography provides spatially resolved surface temperature maps that capture the evolving thermal footprint across the transition. These measurements quantify how the wall-projected thermal footprint encodes the development of the internal scalar boundary layer under non-equilibrium conditions.

EXPERIMENTAL SETUP

The experiments are conducted in a low-speed subsonic wind tunnel at Stanford University (see Fig. 1). The cross-sectional dimensions of the working test section are $H \times W = 0.762 \times 0.762$ m, with a length of 1.45 m. The wind tunnel is configured as an open-loop facility and can achieve average free-stream velocities (U_∞) in the test section ranging from 2 m/s to 10 m/s. The experimental setup uses the full length of the test section ($L = 1.45$ m) to ensure fully developed flow conditions ($Re_\theta \approx 600$–1300 across $U_\infty = 3.5$–8.5 m/s, estimated from a 1/7-power-law turbulent flat-plate correlation). The heated section consists of a 30 cm wide plate, with wooden insulation blocks placed along the edges to minimize lateral heat loss. The core heating element is an adhesive-mount silicone heater (McMaster-Carr) applied to an insulated base to provide a constant heat flux. A thin copper heat-spreader plate sits above the heater to homogenise the imposed flux, and a replaceable test surface is mounted on top of this assembly. Thermal contact between the heater, the copper heat spreader, and the replaceable test surface is established using Arctic Silver thermal compound to minimise contact resistance and ensure that the prescribed heat flux is delivered uniformly to the surface. The walls of the test section are made of thermally insulated material, and a trip wire is installed to promote boundary layer transition. Two test surfaces are used in this study: a smooth copper plate (0.8 mm thick), and a rough surface assembled from nine individually 3D-printed 100 mm $\times$ 100 mm tiles, each fabricated using Direct Metal Laser Sintering (DMLS) in aluminum–silicon–magnesium (AlSiMg) and joined in a 3×3 grid to form a 300 mm $\times$ 300 mm rough patch. The roughness geometry is chosen to align with the DNS study of Hantsis & Piomelli (2020) and consists of k-type roughness composed of randomly oriented ellipsoids with semi-axes k, $1.4k$, and $2k$, with $k = 0.8$ mm.

A steady-state procedure is used to capture data for calculating the convective heat transfer coefficients. Surface temperatures are measured with a FLIR A325sc thermo-vision IR camera fitted with a 10 mm lens, producing a 320×240 pixel temperature map over a viewing area of 0.45×0.62 m. The silicone heater is operated at nominal heat fluxes between 250 W/m^2 and 1000 W/m^2 across the range of freestream velocities tested for both smooth and rough configurations. Prior to each run, a no-flow steady-state thermal image is acquired with the heater on and the tunnel off to confirm that the imposed heat flux is uniformly distributed across the test surface. The freestream flow is then established and the system is then monitored until thermal steady state is achieved, which typi-

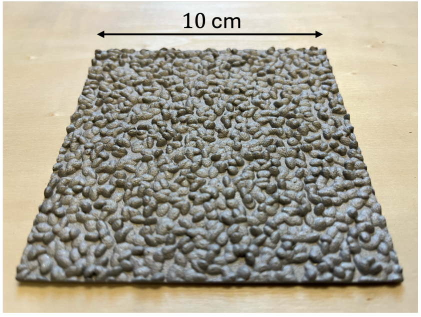

Figure 2: Photograph of a single 3D-printed roughness tile (DMLS, AlSiMg), showing the as-fabricated surface texture.

cally requires two hours of continuous operation, after which temperature data are recorded for 30 seconds at 10 Hz. This procedure is repeated for both surface configurations.

The local convective heat transfer coefficient is recovered by accounting for radiative losses from the heated surface at each pixel. Because the radiative loss depends on the local wall temperature, which in turn depends on the convective flux through the boundary layer adjustment, the energy balance is solved iteratively: an initial estimate of $T_w(x,z)$ is used to compute the radiative loss and the corresponding convective flux, and the wall temperature is updated until convergence.

RESULTS

Figure 3 presents steady-state surface temperature contours measured via infrared thermography for both smooth and rough configurations at $U_\infty = 8.5$ m/s and $q'' = 1000$ W/m^2 (panels (a)–(b)), together with rough-surface measurements at four lower freestream velocities (panels (c)–(f)). The smooth-wall field (panel a) exhibits a pronounced streamwise temperature gradient characteristic of a thermally developing boundary layer, with the highest wall temperatures near the leading edge of the heated section decaying toward the trailing edge. In contrast, the rough-wall temperature contour at the same velocity (panel b) is markedly more uniform in the streamwise direction, indicating enhanced convective mixing that reduces wall temperature rise along the entire heated patch. From the measured wall temperatures, the local Stanton number and streamwise Reynolds number are computed at each pixel as

$$St = \frac{q''_{\text{conv}}}{\rho_\infty U_\infty C_p (T_w - T_\infty)}, \qquad Re_x = \frac{U_\infty x}{\nu}. \qquad (1)$$

The centreline St is shown in Fig. 4a and compared against the semi-empirical prediction for a turbulent boundary layer with an unheated starting length correction (Ambrok, 1957):

$$St = 0.0308\, Re_x^{-1/5}\, Pr^{-2/3} \left[1 - (\xi/x)^{9/10}\right]^{-1/9}, \qquad (2)$$

where ξ is the unheated starting length and Pr is the Prandtl number.

The Stanton numbers are consistently elevated on the rough surface relative to both the smooth-wall measurements and the semi-empirical prediction of Eq. (2). The elevation persists across the full range of Reynolds numbers examined, confirming that surface roughness augments convective heat transfer beyond the smooth-wall baseline and beyond what semi-empirical correlations accounting only for Reynolds number dependence would predict. The elevation is consistent with the DNS results of Hantsis & Piomelli (2020), who showed that roughness introduces a pressure-drag mechanism that enhances momentum transfer more than scalar transfer. Closer inspection of the rough-wall contours reveals faint residual patterning from the 3×3 tile assembly, visible as mild temperature variations aligned with the tile joins. These features reflect small tile-to-tile variations from the assembly process and differences in local thermal contact at the joins and their amplitude is within the experimental uncertainty of the measurements.

Panels (c)–(f) of Fig. 3 show the effect of freestream velocity on the rough-surface temperature field at constant $q'' = 1000$ W/m^2. As U_∞ increases, the wall temperature decreases and the streamwise gradient flattens. At lower velocities the surface imprint is more pronounced and extends further downstream: wall-normal turbulent mixing redistributes thermal energy from the heated wall into the boundary layer, and streamwise momentum advects this thermally-loaded fluid downstream, so the wall imprint retains the upstream thermal memory of the outer layer over an extended fetch (Li *et al.*, 2019).

Figure 4b shows the centreline mean temperature excess $\Delta T(x) = \overline{T}_w(x) - T_\infty$ extending through and beyond the heated patch. A distinct thermal imprint persists downstream of the trailing edge of the rough heated region over a distance of approximately 50 mm, decaying gradually rather than returning abruptly to the freestream level. Because the copper heat spreader terminates at the trailing edge of the heater and the downstream wall comprises thermally insulating material, streamwise conduction through the substrate into the downstream region is strongly suppressed; the persistence observed in the IR field is therefore convection-driven, reflecting the conjugate coupling between the heated fluid and the downstream adiabatic wall rather than solid-side conduction from the heated region. This persistence is indicative of a scalar field that has not re-equilibrated to the downstream surface conditions within the measurement domain. MacDonald (2024) reported from DNS that the recovery length depends on both the direction of the transition and the quantity considered: for momentum, the rough-to-smooth adjustment reaches equilibrium within approximately $1\,\delta$, compared with $2\,\delta$ for the smooth-to-rough case, whereas the scalar-flux recovery requires of order $3\,\delta$ in both directions, systematically longer than the momentum recovery. The residual temperature wake observed here is qualitatively consistent with this asymmetry: the thermal field has not re-established equilibrium with the local (unheated, smooth) wall conditions within the measurement domain. Jensen & Forooghi (2025) similarly found that full equilibrium after a step change in surface conditions requires a downstream distance of order 8δ, with secondary motions and dispersive stresses sustaining non-equilibrium at smaller scales.

Beyond the bulk heat-transfer enhancement, the surface temperature field also encodes how the roughness geometry imprints on the wall. The time-averaged temperature is decomposed as $\bar{T}_w(x,z) = \langle \bar{T}_w \rangle_z(x) + \tilde{T}(x,z)$, where $\langle\cdot\rangle_z$ is the spanwise average and $\tilde{T}$ is the dispersive deviation. By construction, $\tilde{T} \equiv 0$ on a homogeneous surface, so any organised structure in $\tilde{T}$ reflects the underlying surface heterogeneity. Figure 5(a) shows $\tilde{T}(x,z)$ over the rough patch at $U_\infty = 8.5$ m/s and $q'' = 1000$ W/m^2, and Figure 5(b) shows the corresponding surface height map $k(x,z)$ of the 3×3 tile assembly at the

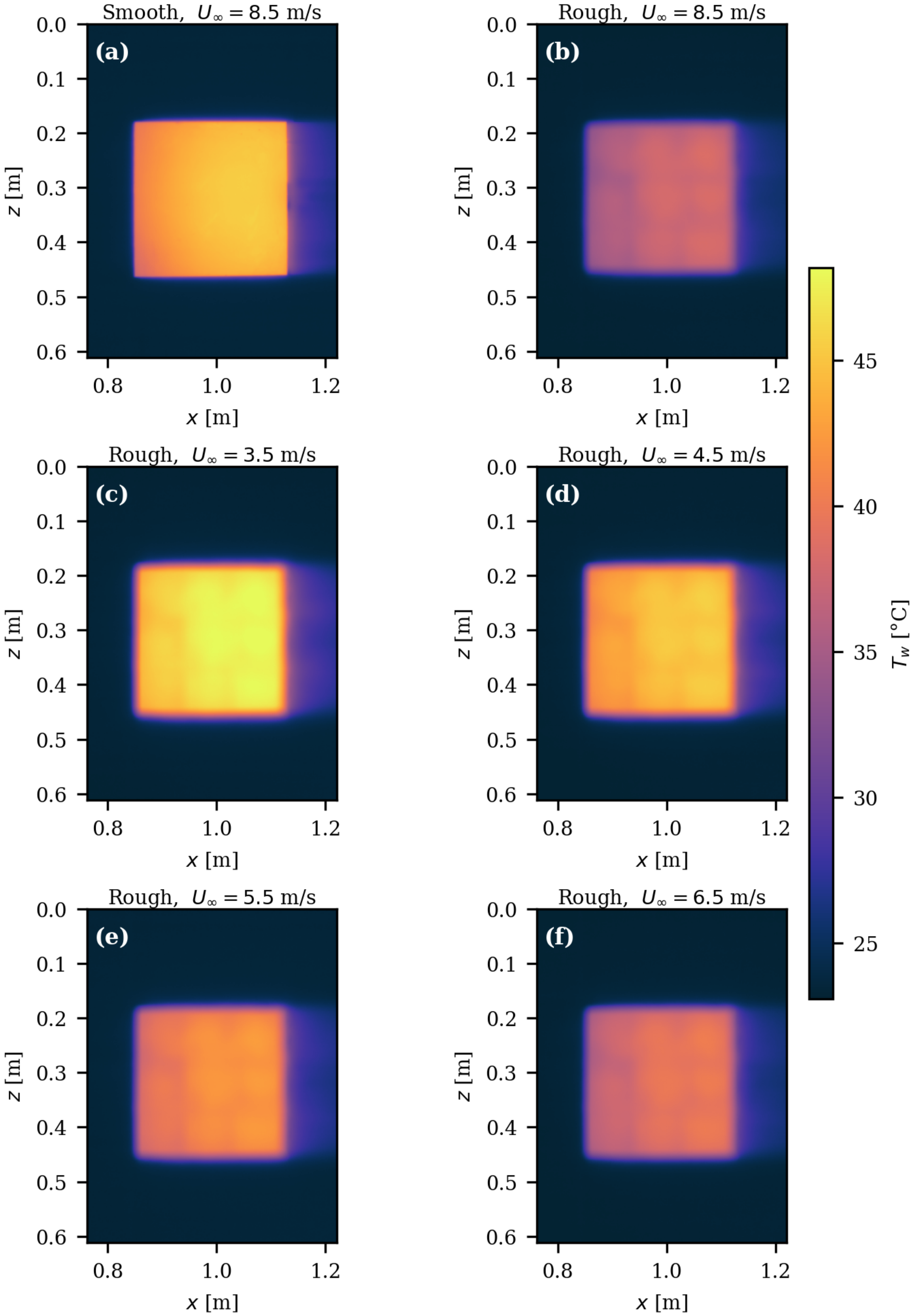

Figure 3: Steady-state mean surface temperature T_w at $q'' = 1000$ W/m^2. (a) Smooth, $U_\infty = 8.5$ m/s; (b) Rough, $U_\infty = 8.5$ m/s; (c) Rough, $U_\infty = 3.5$ m/s; (d) Rough, $U_\infty = 4.5$ m/s; (e) Rough, $U_\infty = 5.5$ m/s; (f) Rough, $U_\infty = 6.5$ m/s. Shared colorbar.

same spatial scale. Two mechanisms appear to shape this footprint. First, the local heat transfer coefficient $h(x,z)$ is expected to reflect the roughness geometry through impingement on windward faces, recirculation in leeward cavities, and shel-

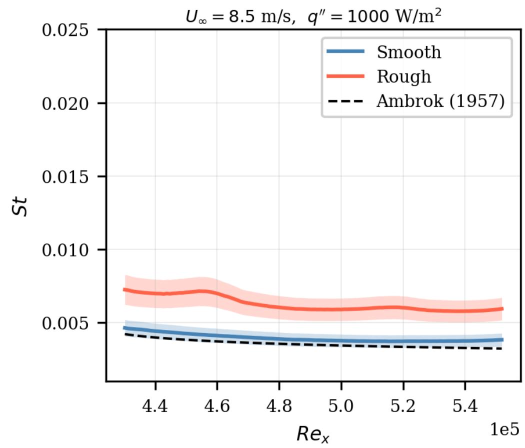

(a) Centreline Stanton number *St* vs. Re_x for smooth and rough surfaces at $U_\infty = 8.5$ m/s, with Ambrok (1957) flat-plate prediction.

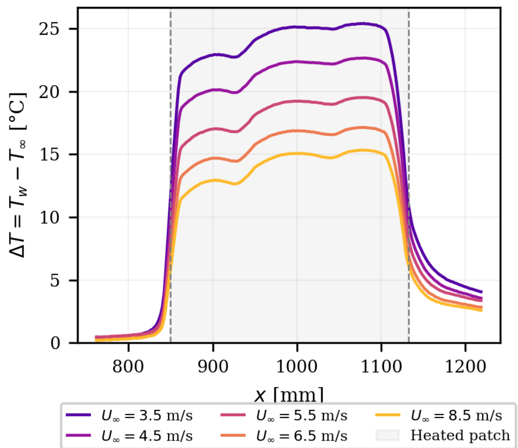

(b) Centreline temperature excess $\Delta T = \overline{T}_w - T_\infty$ vs. streamwise position, rough surface, all velocities.

Figure 4: Summary of heat transfer results at $q'' = 1000$ W/m^2.

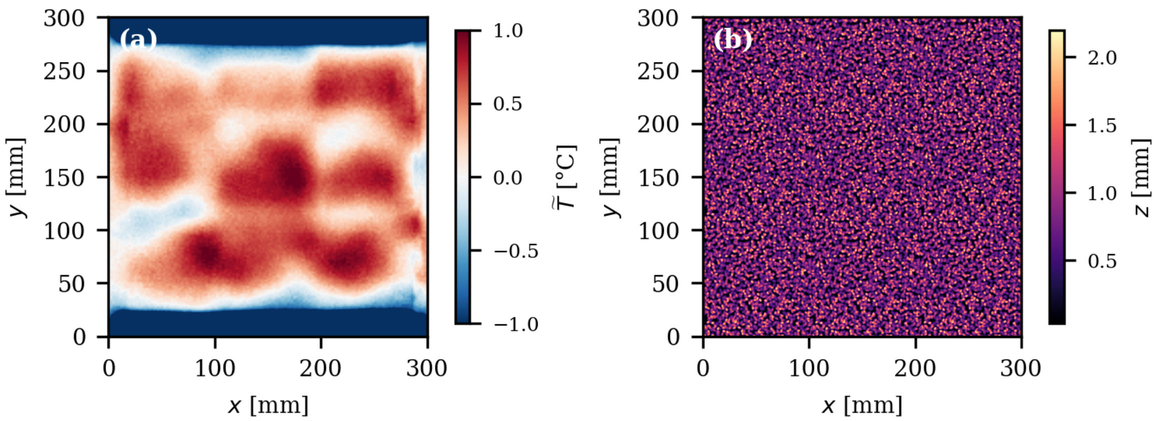

Figure 5: (a) Dispersive wall temperature $\widetilde{T}(x,z) = \overline{T}_w - \langle \overline{T}_w \rangle_z$ and (b) roughness surface elevation (3×3 tiled Piomelli geometry), for the rough surface at $U_\infty = 8.5$ m/s over the same 300 mm $\times$ 300 mm footprint.

tering behind taller elements, so spatial variations in h at fixed wall heat flux would translate into corresponding variations in $\tilde{T}$. This geometric modulation is the surface-observable counterpart of the form-induced (dispersive) contribution to scalar transport in the double-averaged formulation (Hantsis & Piomelli, 2020), in which the spatial correlation between wake-field velocity and wake-field temperature generates a mean wall-normal flux, and can contribute a significant fraction of the total scalar transport within the roughness sublayer. Second, the AlSiMg substrate has finite thermal conductivity, so solid-side conduction redistributes heat within the rough elements before it reaches the fluid-side surface, modifying the local temperature distribution relative to the idealised iso-flux case (Stroh *et al.*, 2025). The measured $\tilde{T}$ therefore appears to blend a geometry-driven fluid-side signature with a conjugate solid-side response. Resolving these contributions, and in particular directly quantifying the form-induced heat flux at the wall, is a natural next step that would require concurrent velocity measurements within the roughness sublayer. At the present IR resolution of $\sim$1.9 mm/pixel with $k = 0.8$ mm, element-scale interactions are unresolved, so $\tilde{T}$ is best interpreted as the wall-projected footprint of the roughness topography. Together, the elevated Stanton numbers, the persistent downstream thermal footprint, and the dispersive temperature field reflect a coupled scalar-roughness interaction in which conjugate heat transfer shapes the wall thermal response.

SUMMARY AND OUTLOOK

Surface roughness enhances convective heat transfer and elevates Stanton numbers above smooth-wall and semi-empirical predictions. A thermal footprint persists downstream of the heated rough patch over approximately 50 mm, suggesting that the scalar field has not re-equilibrated to the downstream surface conditions within the measurement domain. DNS results by MacDonald (2024) and Jensen & Forooghi (2025) indicate that scalar recovery lags momentum recovery following roughness transitions, and the present surface measurements are qualitatively consistent with this picture. The dispersive temperature field further reveals roughness-geometry imprinting at the wall. To directly quantify the differential development of scalar and momentum internal boundary layers, future work will introduce wall-normal cold-wire thermometry to extract the scalar IBL thickness $\delta_\theta(x)$ and turbulent heat flux $\langle T'v' \rangle(y)$ at stations spanning the transition, paired with concurrent hot-wire anemometry and time-resolved IR thermography (Foroozan *et al.*, 2025).

Acknowledgment

Support from the Office of Naval Research to the Center for Turbulence Research (grant N000142312833) is gratefully acknowledged.

REFERENCES

Abe, H., Kawamura, H. & Matsuo, Y. 2004 Surface heat-flux fluctuations in a turbulent channel flow up to $Re_\tau = 1020$ with $Pr = 0.025$ and 0.71. *Int. J. Heat Fluid Flow* **25**, 404–419.

Ambrok, G. S. 1957 Approximate solution of equations for the thermal boundary layer with variations in boundary layer structure. *Soviet Phys. Tech. Phys.* **2** (9), 1979–1986.

Foroozan, F., Ianiro, A., Discetti, S. & Baars, W. J. 2025 Resolving convective velocities of turbulent boundary layer–induced convective heat transfer fluctuations at the wall. *Phys. Rev. Fluids* **10**, 094904.

Hantsis, Z. & Piomelli, U. 2020 Roughness effects on scalar transport. *Phys. Rev. Fluids* **5**, 114607.

Jensen, R. M. & Forooghi, P. 2025 A study of turbulent flow over patchy roughness. *J. Fluid Mech.* **1006**, A28.

Kadivar, M., Tormey, D. & McGranaghan, G. 2021 A review on turbulent flow over rough surfaces: fundamentals and theories. *Int. J. Thermofluids* **10**, 100077.

Li, M., de Silva, C. M., Chung, D., Pullin, D. I., Marusic, I. & Hutchins, N. 2019 Recovery of wall-shear stress to equilibrium flow conditions after a rough-to-smooth step change in turbulent boundary layers. *J. Fluid Mech.* **872**, 472–491.

MacDonald, M. 2024 Direct numerical simulation of momentum and scalar internal boundary layers. *Int. J. Heat Fluid Flow* **106**, 109285.

Miyake, M. 1965 Transformation of the atmospheric boundary layer over inhomogeneous surfaces. *Tech. Rep.* Defense Technical Information Center.

Rouhi, A., Chung, D. & Hutchins, N. 2019 Direct numerical simulation of open-channel flow over smooth-to-rough and rough-to-smooth step changes. *J. Fluid Mech.* **866**, 450–486.

Stroh, A., Secchi, F. & Garg, H. 2025 Effects of conjugate heat transfer on the thermal properties of turbulent flow over rough walls. In *Proc. 11th Int. Symp. on Turbulence, Heat and Mass Transfer (THMT-25)*. Tokyo, Japan, paper DNS-HT-1-05.